0G TESTING OF ALTERNATIVE BOOM ROOT INTERFACE CONCEPTS FOR ROLLABLE COMPOSITE BOOMS

Marco Straubel [(1)], Martin F. Hillebrandt [(1)]

[(1)] DLR Institute of Lightweight Systems, Lightweight Design Department, Lilienthalplatz 7, 38108 Braunschweig, GERMANY, Emails: marco.straubel@dlr.de and martin.hillebrandt@dlr.de

KEYWORDS

Deployable structures, composites, mechanisms, kinematics, parabolic flight.

ABSTRACT

In July 2021, DLR conducted a test campaign in artificial weightlessness to verify some of its concepts. During this dedicated flight day, the entire 20 m x 5 m test area of the special Airbus A310 was available for 5 experiments in the field of deployable high strain composite space structures.

The results presented here originate from experiment No. 4 in which two different deployment mechanisms for DLR's deployable CFRP masts were tested. Both types of mechanisms use new interface concepts to attach the booms to the satellite structure with high stiffness during and after deployment. Both concepts were extensively evaluated in artificial weightlessness with respect to their safe deployment and stowage as well as their resulting interface stiffness.

The test setup in the aircraft, the test plan and the test procedure are described hereunder. The results are discussed and recommendations are given for the further development of the boom and mechanisms as well as the testing of such structures in artificial weightlessness.

Figure 1: Rollable DLR -Booms in various cross section versions

1. INTRODUCTION

The DLR Institute of Lightweight Systems* has developed a large number of concepts for deployable space structures for versatile applications [1]. All of them rely on so-called high strain composites. This category of deployable structures utilizes elastically deformed thin composite shells instead of hinges to fold the structure for a space saving space transport. The majority of the concept is based on DLR's rollable CFRP masts (see Figure 1) and dedicated deployment control mechanisms developed, built and tested in-house.

1.1. Motivation

The mast design, sizing, analysis and manufacturing has been researched for decades at DLR and have reached a high level of technical maturity. However, the more the understanding of the booms themselves grew, the clearer it became that the performance of each perfectly tuned boom could easily be reduced by a factor of 2 or more if the interfaces between boom and satellite were poorly designed.

This is primarily affecting the local bending stiffness and strength around the x-axis (see axis definition in Figure 2. As secondary effects of this local reductions, the global stability and stiffness is reduced as well.

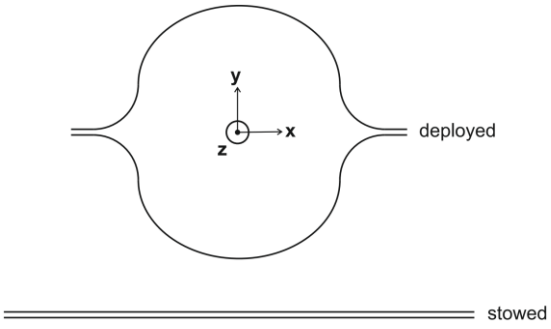

Figure 2: Boom cross sections in deployed and stowed state with reference coordinate system definition

* former DLR Institute of Composite Structures and Adaptive Systems, renamed in January 2023

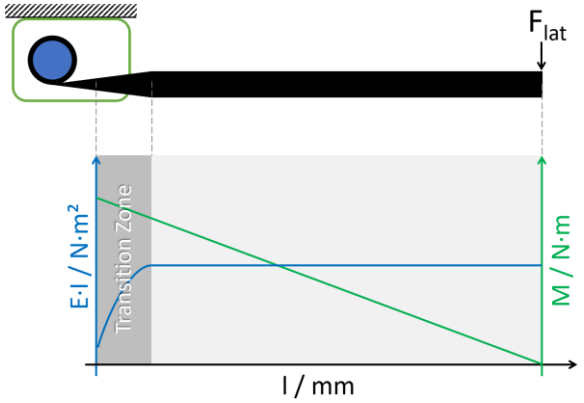

Figure 3: Visualization of coinciding positions of weakened transition zone and highest bending load

1.2. The Challenge

The reason for such severe knock-down factor is visualized in Figure 3. The upper part of the figure shows a schematic boom deployment mechanism (green frame) attached to its host-spacecraft, a boom (black) and the boom spool (blue). The lower part of the figure shows the approximated curves of the bending stiffness EI around the booms x-axis (blue graph) and a bending torque *M* resulting from a generic laterally acting load F_{lat} (load in y-direction, bending moment around x-axis, green graph). The critical region along a partially or fully deployed and loaded boom is the so-called *Transition Zone* which marks the section of the boom where it is no longer coiled onto the boom spool but the cross section has also not fully opened up.

The bending stiffness in the *Transition Zone* is significantly decreased. Furthermore, the bending torque *M* reaches its maximum at the point of maximum distance to the causing lateral load. Consequently, the highest bending load on the mast is generated at the weakest section of it.

This weak interface between boom and spacecraft also generates drawbacks for global column buckling resulting from compression or combined compression and bending loads. To understand this weakening, one need to understand that the decrease in *Bending Stiffness* EI is solely resulting from the cross-section depending *Geometrical Moment of Inertia* I. The relation between the level of cross-section deployment and *I* is highly non-linear. For a stowed boom the relevant cross-section width in y-direction is reduced by some orders of magnitude while the relevant cross-section width in x-direction is even slight increased.

Additionally, the bending strength in this zone is also decreased as a combination of higher tension in the compression-loaded boom shell due to reduced distance between this shell and the neutral fibre and the lower buckling load of the compression-loaded shell due to the wider cross section with resulting increased cross section contour radii. Even worse, when loaded with a too high lateral load the booms cross section tends to flatten itself and can even collapse fully.

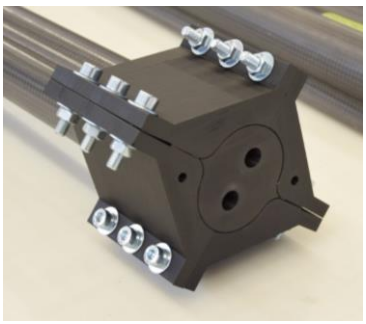

Figure 4: Ideal, solid boom interface for laboratory stiffness testing

1.3. Approach

Interfacing a root deployed boom at its root without the negative effects of a transition zone is only possible under laboratory conditions with stiff, custom-built clamping blocks (see Figure 4). Since the booms deform their cross-section during deployment, such clamping blocks cannot be used in combination with deployment mechanisms.

The only known concept that could use pretty solid interfaces at are so called *Tip-Deployment Concepts*. These concepts fix the free tip of the boom to the spacecraft and use a mobile deployment unit that is moving away from the spacecraft while deploying the boom. This leads to a high tip mass due to the deployment mechanisms at the tip but could - when combined with a jettison-functionality - result in a very light, deployed structure. The resulting debris creation wouldn't be acceptable for usual Earth orbits but could be applicable to interplanetary mission with high demands in mass reduction for example to increase the acceleration resulting from a given electric propulsion system. More detailed thoughts on that are described in [2].

Apart from such concepts, it must be acknowledged that it will be difficult to design a mast support for the mast outlet of a deployment mechanism that offers similar performance to the ideal interface.
In the following, two concepts are presented that attempt to approach this optimum.
Both concepts were tested in a parabolic flight in summer 2021. The focus of these tests was on functional tests to show that all important sub-mechanisms function properly in weightlessness. In addition, vibration decay tests were carried out, which provide information about the stiffness achieved by evaluating the vibration frequency.

2. NOVEL BOOM INTERFACE CONCEPTS

The following section introduce the two most advanced boom root interface concepts. Core

concepts of both systems are protected by already granted [3] or applied patents [4].

2.1. Concept A - The Floating Core

Concept A supports the boom transition zone by a combination of two outer guiding half-shells and one inner core (see Figure 5 and Figure 6). There is only a small gap between the shells and the core through which the boom can pass when extending and stowing. While a movement of the boom shell in longitudinal direction is possible, the interface hinders all movement of the boom shells in lateral direction. Hence, the boom cross section can't be modified and consequently the boom cannot collapse. This concept provides an excellent way of supporting the boom during deployment and in its final deployed state.

More detail can be studied in a dedicated paper by Hillebrandt et al. [5].

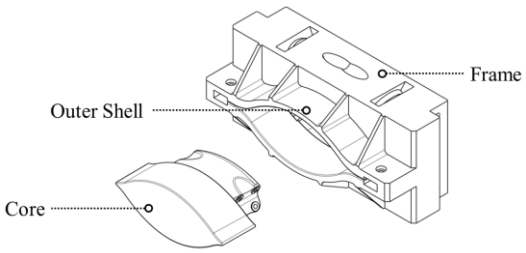

Figure 5: Visualization of the floating core principle used for Concept A [6]

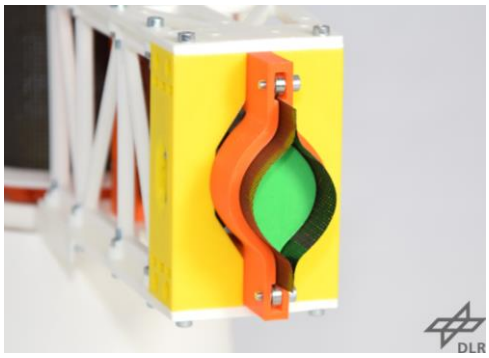

Figure 6: Visualization of the floating core principle used for Concept A [6]

2.2. Concept B - The Deploying Root

In contrast, *Concept B* is not trying to support the boom in its transition zone but to avoid the existence of such a zone. It uses an additional mechanism inside the boom spool to fully open up the boom cross section at the end of the longitudinal boom deployment. This results in a very advanced stiffness and strength behaviour for a fully deployed boom but also limits the possibilities for a good boom support during deployment. Thus, this concept is suited for applications that do not required high loads during deployment but required high mechanical performance once deployed.

The key principle of *Concept B* is relying on two main-functions that are realized in an integrated approach:

I. Deploying the boom root (the segment of the boom that is directly connected to the boom spool) by a boom spool integrated mechanism
II. Locking the boom spool into the sidewalls of the mechanisms housing to prevent further rotation of the boom spool and thereby a pivoting of the boom that is then fixed to the boom spool

Figure 7 shows such a boom spool with integrated mechanism in deployed state.

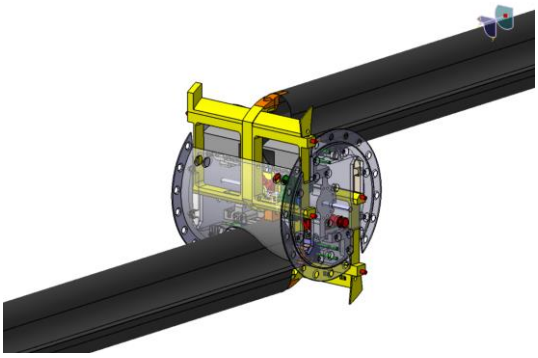

Figure 7: A single boom spool implementing Concept B for a deployment mechanism able to deploy 2 booms with $180°$ offset

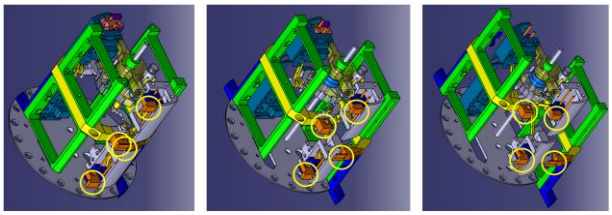

Figure 8: Inner boom spool deployment sequence of Concept B for fully stowed (left), partially deployed (middle) and fully deployed (right) configuration

Figure 8 briefly introduces the inner mechanism installed in the boom spool. The three sub-figures show 3 different stages of deployment. The four yellow circles mark the boom interface brackets (orange) that are the only parts that are in contact to the boom. Those brackets are attached to the boom spool by screws. The brackets are attached to the boom by an appropriate adhesive aided by a custom-made rig.

During the unfolding process of the boom root, these interface brackets change position to mimic the natural cross-sectional change of the boom. Parallel to this cross-sectional deployment, bolts integrated into the green rectangular frames lock the boom spool inside the outer mechanism body.

Table 1 Concept comparison

	Concept A	*Concept B*
Pros	• High bending stiffness and strength during deployment and in deployed state. • Boom spool cavity empty and thus usable by other components. • Simple concepts with passive mechanisms. • Boom can be retracted again after full deployment.	• Very High bending stiffness and strength in deployed state nearly exploiting the fully capability of the boom's stiffness and strength. • Minimum friction at guiding surfaces. • Compact design.
Cons	• Increased friction between boom and guiding surfaces requiring higher motor torque budget. • Not exploiting the fully capability of the boom's stiffness and strength. • Required extra volume and mass for floating core interface outside the main envelope.	• Additional complex mechanisms. • Boom spool cavity is filled with mechanisms and is not available for other components. • Root deployment is a one-shot mechanism that would not allow for an on-orbit retraction.

Many more details on this concept like the used actuator as well as the trigger-concept are described in a dedicated paper by Straubel et al. [7].

2.3. Concept Comparison

Both concepts have their pros and cons that are listed below in Table 1.

The choice of the optimal concept for a dedicated deployable application depends on the boundary conditions of this scenario. *Concept A* seems to be less complex and universal while *Concept B* might be suitable for some mechanically very performance demanding application that can accept the added complexity and the blocked volume in the boom spool cavity. Applications that could fit those properties are instrument booms, solar arrays or solar sails.

Figure 9: Boom deployment mechanism demonstrating Concept A

On the other hand, *Concept B* does not require the large floating core unit that also needs to be located at minimal distance to the boom spool to allow the boom to open up sufficiently.

3. TESTED MECHANISMS

Figure 9 and Figure 10 show the actual hardware tested in flight. For both demonstrators the structural components are mainly 3D-printed but some core components are machined out of aluminium and steel. Standard parts like motors, sensors, ball bearings, springs, screws and nuts are used as well.

This hybrid approach has proven to be very practical and, above all, extremely fast in the last few years of prototype development. On the one hand, the low stresses on the mechanical components of the mechanisms allow the use of plastic components. On the other hand, the use of low-cost FDM printers in-house allows for an enormously fast iteration of the design. Small detailed solutions could thus sometimes go through 2-3 iterations on the same day.

Concept A is driven by a simple brushed DC gear motor. The deployment and stowage of the boom can be realized by simply changing the motor direction.

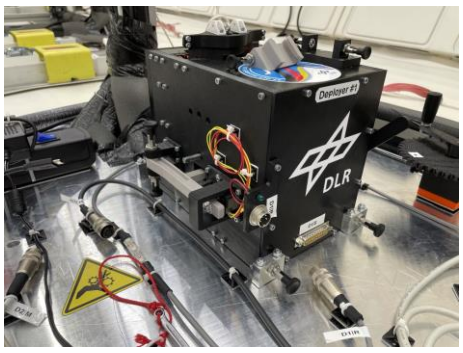

Figure 10: Boom deployment mechanism demonstrating Concept B

Concept B is driven by an advanced brushless DC gear motor and is also equipped with a space-grade launch lock actuator. This prototype was

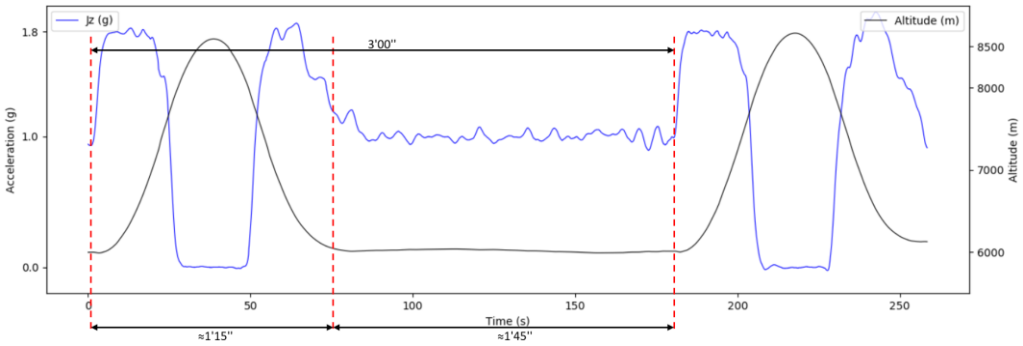

Figure 11: Flight altitude and g-level during and between parabola maneuver (Source: NOVESPACE)

furthermore equipped with a force sensor, a rotary encoder and some end-stop switches.
As the mechanism inside the boom spool requires a manual reset by an operator, only the deployment of this concept was considered a test while the stowing was defined to be a refurbishment activity.

4. TEST OBJECTIVES

The basic motivation of the test was to demonstrate the deployment and stowing of both concepts in relevant environment to help to further mature both designs, increase the TRL and pave the way for future in orbit tests.

A secondary objective was a brief modal survey to characterize their bending stiffness. For *Concept B* those tests were conducted each before and after triggering the boom root cross section deployment kinematic. For *Concept A* only the deployed configuration has been tested.

Thus, the following objectives were defined:

- Concept A
  - I. Demonstrate motorized deployment of the boom and observe the proper behaviour of the deployment mechanism.
  - II. Demonstrate motorized direction change from deployment to retraction of the boom and observe the proper behaviour of the deployment mechanism.
  - III. Demonstrate motorized retraction of the boom and observe the proper behaviour of the deployment mechanism.
  - IV. Validate bending stiffness x- and y-direction at fully deployed state by manually excited swing-out tests.

- Concept B
  - I. Demonstrate motorized deployment of the boom and observe the proper behaviour of the deployment mechanism
  - II. Demonstrate electrically triggered boom root deployment and observe the proper behaviour of the mechanism
  - III. Validate bending stiffness x- and y-direction by manually excited swing-out tests for longitudinal fully deployed boom without deployed boom root.
  - IV. Validate bending stiffness x- and y-direction by manually excited swing-out tests for longitudinal fully deployed boom with deployed boom root.

5. TEST ENVIRONMENT

Both prototypes where tested within DLR's 37th parabolic flight campaign in 2021. As usual for DLR campaigns, this flight was operated by the French company NOVESPACE†. DLR usually conducts 1 to 2 campaigns per year. For the most campaign the $20m$ by $5m$ test area is divided into about 12 - 16 smaller test areas for the same number of individual tests. In this configuration, the aircraft completes one flight each with 30 test parabolas on three consecutive days providing each group of scientists with 90 test-parabolas.

The flight plan for a normal flight day consists of 31 parabolas, whereby the first parabola (parabola #0) is intended for the familiarisation of the experimenters and the pilots and no experiments are carried out in it. The experiments start from parabola #1. There are 6 sets with 5 parabolas each and breaks of about 90 seconds between the individual parabolas. Between each set of 5 there are longer breaks between 5 and 8 minutes. During the breaks, the machine is in cruise flight and the operators can prepare their experiments for the next set.
Figure 11 shows the original sensor data of two consecutive parabolas and the short break in between. The black line represents the course of the flight altitude, the blue curve the g-level. It The altitude is varying between $6000m$ in cruise flight and $8500m$ at the top of the parabola.

Each manoeuvre is split into 4 phases:

1. Pull-Up from second 0 till 20: Aircraft is pulled up to follow the first lower part of the parabola until an upward pitch of about $45°$ is met. Increased g-levels up to $1.8g$ are present within the aircraft.

† https://www.airzerog.com

2. Phase of weightlessness from second 22 till 45: Aircraft is following the upper part of the parabola.
3. Pull-Out from second 47 till 75: Aircraft is pulled out of its $45°$ dive until it is back to $0°$ pitch. Increased g-levels up to $1.8g$ are present again within the aircraft.
4. Cruise flight for about 90 seconds.

Figure 12: Impression of the cabin in flight

Because the three parallel acting pilots have to stabilize the g-level in all three spatial direction manually, the first 2 to 4 seconds of phase 2 cannot be used for sensitive experiments. Therefore, each parabola provides between 18 and 20 seconds of proper so-called *Micro-Gravity*. During this time span the following requirement are met:

- vertical axis: $|a_z| < 0.02g$
- longitudinal axis: $|a_x| < 0.01g$
- lateral axis: $|a_y| < 0.01g$

Particularly because of the one 16m long and the one smaller experiment of a DLR-NASA cooperation project, it was decided to include an additional fourth day in the flight plan. A total of 5 experiments were on board on this flight day, all from the specialist area of deployable space structures. Three of them tested boom deployment mechanisms or their applications [6,8], one demonstrated a new bio-inspired structurally supported deployable membrane [9] and one was dedicated to post-test of tape hinges launched in 2018 on the DLR satellite Eu:CROPIS for solar array deployment.

In total, 18 operators were required to carry out the experiments. The majority were contributed by DLR. Due to the aforementioned DLR-NASA cooperation, two NASA partners were joining the flight. In the spirit of promoting young talent, 3 of the 16 DLR operators were former or active students who were involved in the rack designs or integration of one experiment.

Figure 12 shows a single extracted frame of one of the cameras that were filming the entire flight. The experiment described here as well as its 3 operators can be seen in the lower right corner of this picture.

6. TEST SETUP

6.1. Mechanical Setup and Accommodation

Figure 13 shows the setup as finally installed in the test aircraft with labelled parts. The entire setup is bolted onto a 10mm thick solid aluminium plate that is bolted to the aircraft seat rails with 4 massive screws (hidden under the grey foam tubing at the base plate edges).
In this figure the *Concept B* deployment mechanisms is installed. However, realized by a quick release attachment concept relying on 4 locking-bolts as well as proper electric connectors, the mechanisms of both concepts can be swapped in a few seconds. Both concepts provide identical adapters at the boom tip to accommodate a battery driven camera that should on one hand document the experiment from this perspective and on the other hand provide a constant tip mass for the performed vibration tests.

One very prominent part of the setup is the support mast. It is provided with some pulleys and a thin rope that is used as safety rope to secure the fully or partially deployed boom during the 1.8g phases that take place between the 0g phase. One end of the rope is attached to the boom tip. The other end is basically free and can be controlled by hand by one of the operators. Between the individual parabolas this free end is secured in a rope clamp (sailing equipment). The rope was always well tensioned during all non-0g phases but had sufficient slack during the actual testing at 0g.

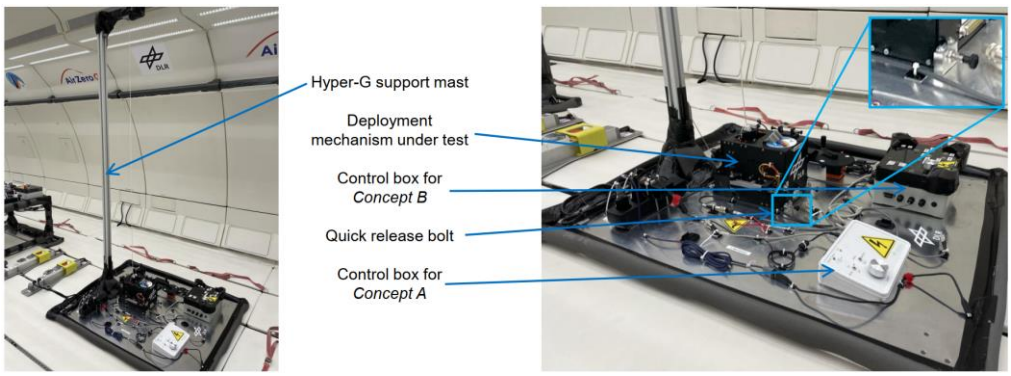

Figure 13: Setup of the test rack in the aircraft.

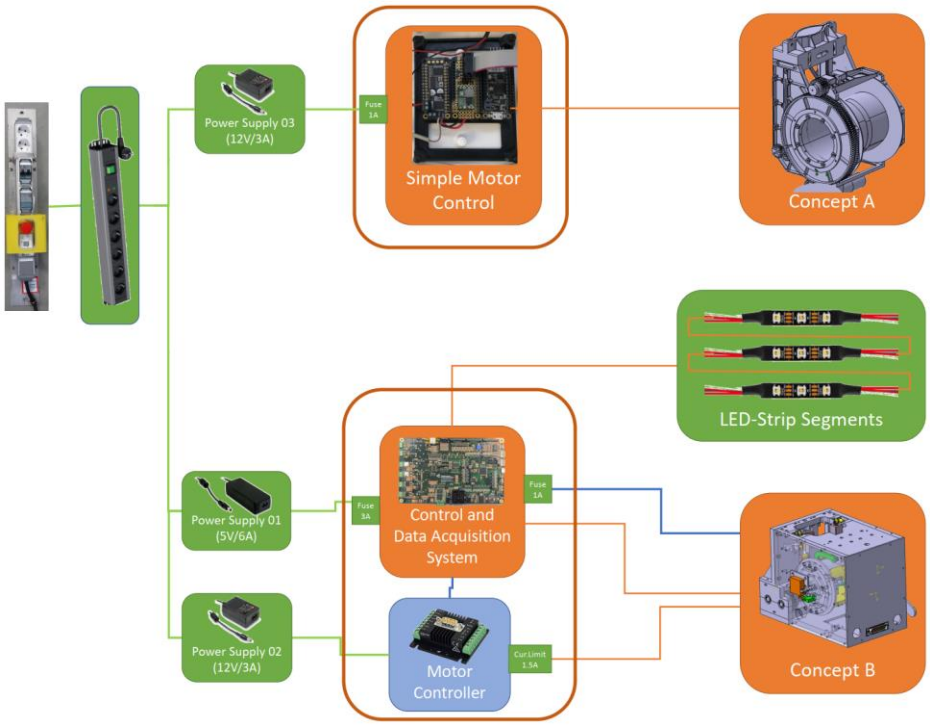

Figure 14: Schematic of the test setup electronics.

6.2. Electric Setup

Figure 14 show the complex electric schematic that was required to operate the setup. Each deployment mechanism is run by its own custom electronics box. Given by the fact that the *Concept B* unit was equipped with more sensors and actuators, the electronics of this model were also more complex. It could deploy the system automatically, stop once the longitudinal deployment is finished and could also trigger the boom root deployment automatically. In parallel it records all relevant sensor data as well as system variables and a time stamp from an included RTC (real time clock) to an included memory card.

This box also controlled three short LED strips that were used to later synchronize the obtained data of the rack-electronics with the camera footage of the observing cameras.
Both controller boxes are filled with Arduino-compatible electronics. The “Simple Motor Controller” in Figure 14 used off-the-shelf components from the DIY-electronics provider Adafruit Industries, LLC (see Figure 15). It consists of an Arduino-compatible microcontroller (SAMD51), a DC-motor driver, a 12V to 5V DC-DC step-down converter as well as a mandatory fuse demanded by NOVESPACE for safety reasons. For a proper user interface, different switches, LEDs and a potentiometer where installed in the top lid. The embedded software on the microcontroller was written by the operators using the *Visual Studio Code* IDE in combination with the *Platform-IO* add-on.

The control electronics of Concept B were much more sophisticated a it reuses an earlier in-house development of an Arduino-compatible PCB with a large set of features. This PCB (see Figure 16) has been develop in order to operate the deployment module of the DLR-NASA deployment mechanisms described to detail in [8].

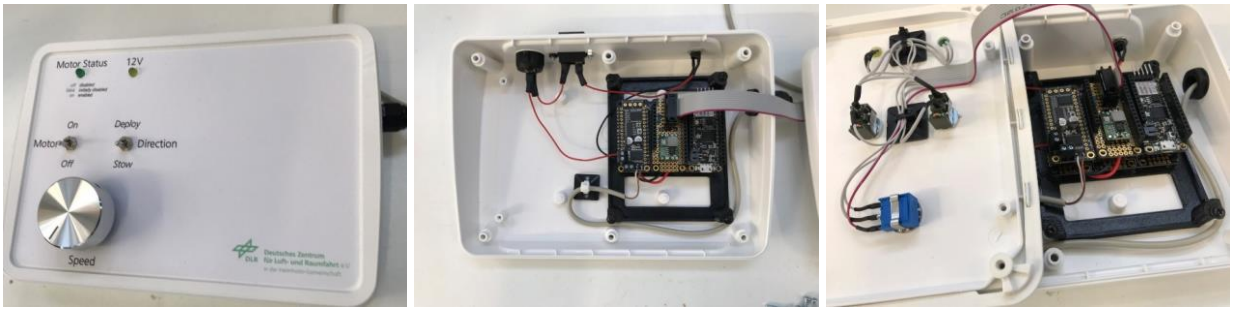

Figure 15: Control electronics of Concept A.

Figure 16: Custom PCB used for Concept B control and data acqusition

The PCB offers the following features:

- Arduino-compatible SAMD21J microcontroller,
- Battery-backed real-time clock (DS3231),
- On-board SD-card slot,
- On-board flash memory,
- Sockets for optional WiFi, Bluetooth or generic 2.4GHz RF modules,
- 8 filtered encoders inputs,
- 5 filtered end-stop inputs,
- 2 alternative power inputs for up to 32VDC for external consumers,
- 4 microcontroller-controlled MOSFETs with individual current monitoring for heaters or HDRMs,
- Monitoring of all relevant input power levels,
- 3 ports for external thermocouple amplifiers,
- External ports for optional external components (3x Serial, 2x I²C, 2x SPI),
- 5 filtered inputs for user buttons,
- Standard connectors for *RepRap Full Graphic Smart Controller*‡ including display, rotary encoder, second SD-Card, speaker and reset button,
- Two analogue inputs for potentiometers,
- Outputs for LEDs (8 standard LEDs via separate on-board PWM controller and one level shifted port for WS-2812-style smart LED stripes),
- One BNO-055 IMU MEMS-sensor.

The embedded software on the microcontroller was written by the operators using the *Microchip Studio* IDE in combination with *Visual Micro* add-on.

6.3. Cameras

In total 2 cameras were installed at the handrails of the aircraft to observe the entire experiment (Figure 17b and Figure 17d). Two cameras were attached to the experiment base plate. One of them focused on the trigger actuator for the boom root deployment (Figure 17a). The second was looking up to the boom tip in order to have a good view on the shaking boom tip during the modal tests (Figure 17e). The fifth camera is the one attached to the boom tip (Figure 17c).

7. TEST PLAN

Table 2 provides insight into the test plan for the flight day. The 30 test parabolas were equally split between both concepts.

7.1. Concept B

Concept B used the first 3 sets of 5 parabolas to basically repeat the same test plan three times. The mast was deployed distributed over 3 parabolas in order to test with representative deployment speed.

In the first part of the fourth parabola of each set, the mast tip of the fully deployed mast was deflected by one of the operators manually and then released. The mast was then given a few seconds to complete up to 5 complete oscillation periods. Depending on the stiffness, between 2 and 6 of these swing-out tests could be performed in a row in one parabola. The operator regularly changed the direction between the individual excitations so that the decay behaviour could be observed in the x- and y-direction.

Towards the end of this parabola, the other operator triggered the deployment of the mast root by the control box. As this sub-mechanism was driven by a relatively powerful pre-tensioned spring, it was completed in a few fractions of a second.

In contrast to *Concept A* the deployment is not stopped by the operator but by the electronics that sensed the end of the longitudinal deployment by an end stop within the deployment mechanism. For this concept it is very vital to stop the deployment at the very correct spot. The boom needs to be fully un-spooled from the spool and the spool need to be in

(a) Cam #1 *(b) Cam #2* *(c) Cam #3* *(d) Cam #4* *(e) Cam #5*

Figure 17: Images taken by all five cameras.

‡ https://reprap.org/wiki/RepRapDiscount_Full_Graphic_Smart_Controller

Table 2 Test Plan

Parabola	*Concept under Test*	*Test Description*
#1	Concept B	Deployment up to 33% length.
#2	Concept B	Deployment up to 66% length.
#3	Concept B	Deployment up to full length.
#4	Concept B	Vibration decay tests followed by triggering of boom root deployment
#5	Concept B	Vibration decay tests after boom root deployment
#6 .. #10	Concept B	Repeating test of parabola #1 to #5.
#11 .. #15	Concept B	Repeating test of parabola #1 to #5.
#16	Concept A	Deployment up to 20% length.
#17	Concept A	Deployment up to 50% length.
#18	Concept A	Deployment up to 80% length.
#19	Concept A	Deployment up to full length.
#20	Concept A	Vibration decay tests.
#21	Concept A	Deployment up to 50% length.
#22	Concept A	Deployment up to full length.
#23	Concept A	Direction switch from deploy to stow and stow approx. 5cm.
#24	Concept A	Stowing down to 50% length.
#25	Concept A	Stowing down to fully stowed.
#26 .. #30	Concept A	Repeating test of parabola #16 to #20.

the correct angular orientation, with respect to the mechanism outer walls, in order to activate the boom root deployment sub-mechanism without damaging the boom and/or jamming the mechanism.

The last parabola of each set was used to repeat the swing-out tests with deployed root mechanism. Again, several swing-out tests could be carried out in different directions.

At the end of each of the first three sets the demonstrator was refurbished to its initial, stowed state. Therefore, the boom root deployment mechanism was reset with an external tool operated by one operator while the deployment motor was running backwards. The triggering release nut launch lock actuator is based on a non-destructive SMA (Shape Memory Alloy) principle. This actuator could be reset very easily by simply pressing the released nut back into its locking cavity.

7.2. Concept A

As *Concept A* was less complex and also able to retract the boom itself, the test plan looks a bit different. With no boom root deployment necessary, the deployment was distributed across 4 parabolas for 2 out of 3 test sets. The fifth parabola was then used for swing-out tests. The refurbishment for the next set was done simply by reversing the drive direction of the motor. As *Concept A* provides a good amount of stiffness in all deployment phases, this could be done under $1g$ cruise flight without any additional support of the boom tip.

In the fifth test set (parabola #21 to #25) the deployment should be done with doubled speed in order to deploy the mast within two parabolas. The third parabola of this set was used to demonstrate the direction change from deployment to stowage under weightlessness. During the last two parabolas the boom was retracted back to the stowed position.

Figure 18: Concept A fully stowed (prior to parabola #16).

8. TEST RESULTS

8.1. Concept A

8.1.1. Proper mechanism operation

The deployment mechanism utilizing *Concept A* was performing absolutely flawless (see Figure 18 and Figure 19). The three deployment tests as well as the one retraction test in microgravity were running smooth no matter if the motor was run faster or slower. Although loaded with a tip mass of $300\ gram$ the boom was never close to buckling even under $1g$ or $1.8g$ load.

Figure 19: Concept A fully deployed (during parabola #20).

After the flight, the mast was thoroughly checked for possible damage and traces of grinding or colour changes. No changes could be detected.
During review of the camera footage it was observed that one operator was unintentionally overloading the boom while manually deflecting it in boom x-direction in order to do the swing-out test (see Figure 20).

The footage shows how a buckle formed at the compressive loaded boom flange during operator manipulation. Once the operator releases the boom to start the swing-out, the buckle popped out by itself. This unintended overload also demonstrates the robustness of the concept and the booms.

8.1.2. Swing-Out tests

The swing-out test were analysed using the free image analysis software *Tracker*[§]. The software is able to examine videos and automatically track points of interest along the single video frames. These points do not have to be special targets but only have to stand out clearly from the background and not move too much between two frames.

In the course of initial pre-processing of the various camera recordings, a combined video was created showing three different scenes on one screen. All partial videos were synchronized with the audio tracks of the individual segments. The clearly audible announcements of the pilot during the flight were used for the synchronisation.
Figure 21 and Figure 22 shows two output of the analysis of this combined video with the *Tracker* software. In both figures the same mentioned video is used as source but the software was advised to track the movements of different features of the video (marked with a yellow circle).
Both analyses show a good vibration decay sequence between $11s$ and $13.5s$. For both spots the movements in horizontal image direction (x-direction) was used for further calculation.

The vibration frequency was derived by selecting a possibly high number of clearly identifiable vibration periods. By determining the time span of this sequence $T_{decay,n}$ and the number of full periods n_{decay} one can calculate the resulting frequency f_A by Eq. (1)

$$f_A = \frac{n_{decay}}{T_{decay,n}} \qquad (1)$$

For the footages of both cameras the following frequencies have been calculated

$$f_{A|Cam4} = 2.66\ Hz \qquad (2)$$

$$f_{A|Cam2} = 2.57\ Hz \qquad (3)$$

As described in section 7, the swing-out test should be performed multiple times and alternating between both boom bending directions. However, it turned out that the bending stiffness around the boom y-axis[**] is significantly increased in contrast to the stiffness around the x-axis. While this is a good point for later applications it led to issues with the used test method for test around the boom y-axis. The boom tip could not be deflected by a noticeable distance without overloading the boom and cause local buckling (see again Figure 20). When loaded properly the resulting vibration was damped strongly and couples into the x-bending vibration after 2 to 3 full oscillations.

The best observed bending around the y-axis can be seen in Figure 21 between $9.1s$ and $10.4s$. However, the characteristic is too unclean and the number of oscillations is too small to derive a frequency from this data.

[§] https://physlets.org/tracker/

[**] please refer again to Figure 2 on page 1 for the coordinate system definition

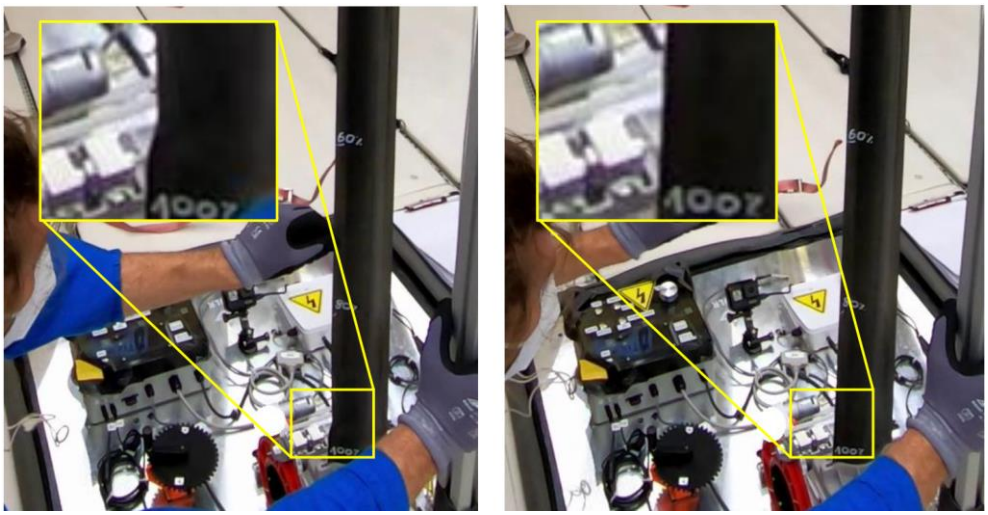

Figure 20: Boom forms buckle at boom flange while overloaded by operator (left). Buckle pops out without damage after release by operator (right).

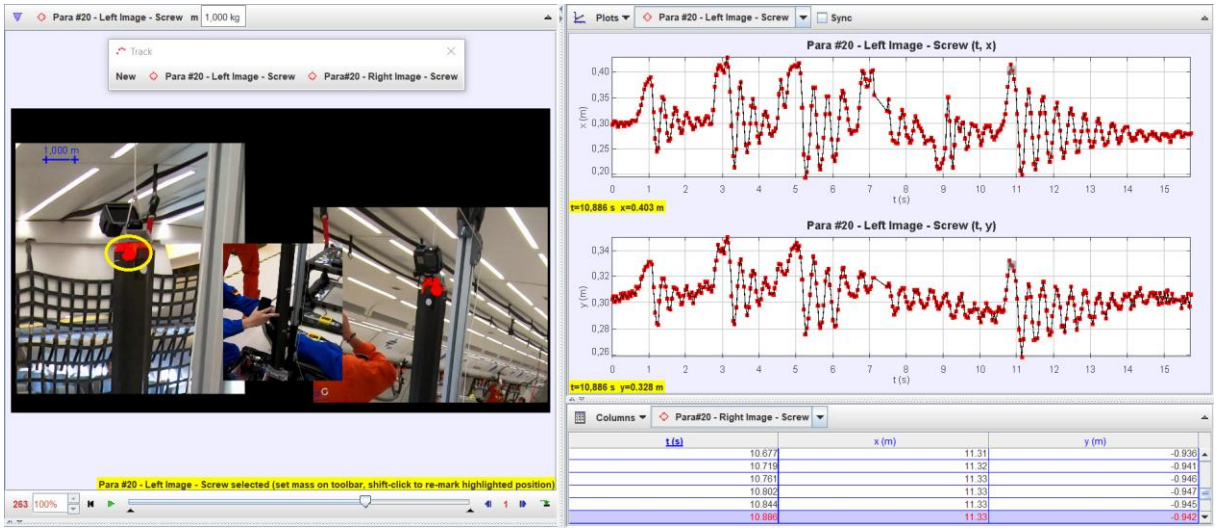

Figure 21: Video analysis of partial footage of Cam #4 during parabola #20.

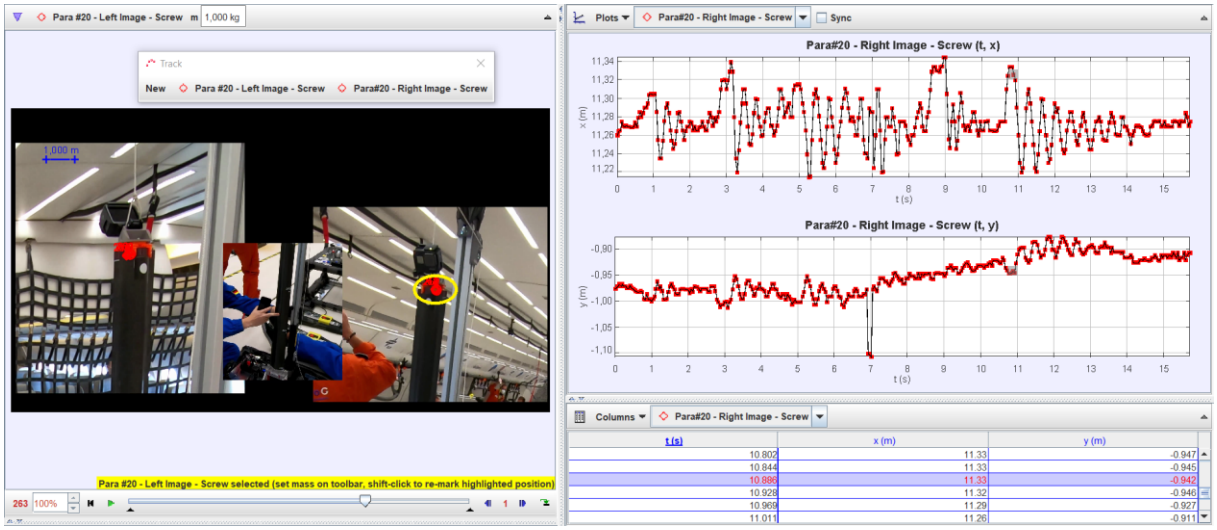

Figure 22: Video analysis of partial footage of Cam #2 during parabola #20.

8.2. Concept B

8.2.1. Proper mechanism operation

On first evaluation, the deployment mechanism utilizing Concept B was performing flawless as well. The three deployment tests in microgravity were performed as planned. This is true for both the longitudinal deployment including automatic stop and the boom root deployment.

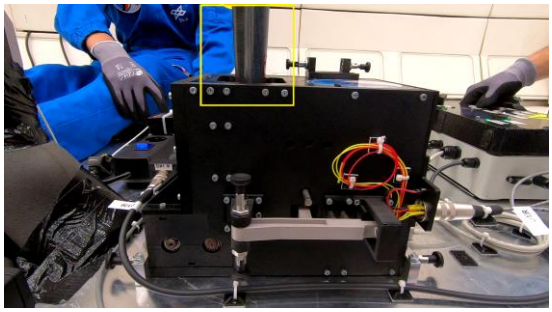

(a) Total field for view of Cam #1

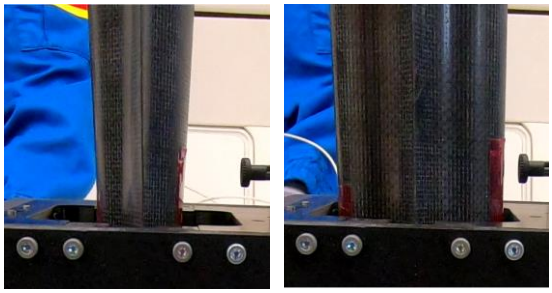

(b) Enlarged view on the boom root before (left) and after (right) the boom root deployment

Figure 23: Boom root deployment in parabola #4

The effect of the boom root deployment is visualized in Figure 23 from the perspective of Cam #1. Figure 23(a) shows an overview frame that was made with a fully deployed boom but un-triggered boom root deployment mechanism. Figure 23(b) shows two enlarged images of the identical setup once before and once after the boom root has been unfolded. It is obvious that the boom is much wider after the triggering of this mechanisms. It can also be seen that the cross-section does not open up further along the entire length as before, but is the same size everywhere.

Regarding the general appearance of the deployment it needs to be stated that the reduced support of the boom *before* the boom root deployment led to a significant decrease in bending stiffness. The deployed portion of the boom was swivelling in positive and negative y-directions by about $\pm 5°$. During deployment and during the swing-out tests such panning also happened spontaneously while there was not obvious reason for this at this point.

It was later understood that this reaction was caused by a short inaccuracy in the micro-g environment that was affecting a relative heavy tip load that was mounted to a boom with limited bending stiffness in its root interface.

While this could be accepted for the later application deployment in space with a true 0g environment it could cause a severe risk for the boom root deployment. If the mast is not well aligned it the moment the root deployment is triggered, the root deployment could jam or - if this sub-mechanism is actuated with enough force - even damage the boom itself. On the other hand, so far, the inner boom deployment mechanism is driven by a preloaded spring. When substituting this actuator with a gear motor, a gentler and possibly even reversible new concept could be generated.

8.2.2. Swing-Out tests

Figure 24 shows results from the conducted analysis of *Concept B* related footage.

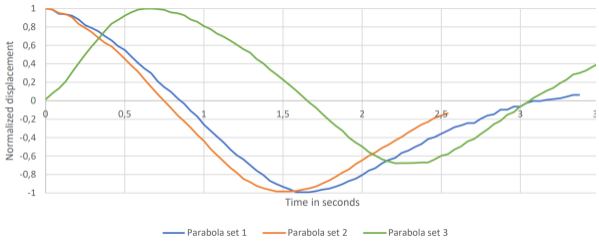

(a) before boom root actuation

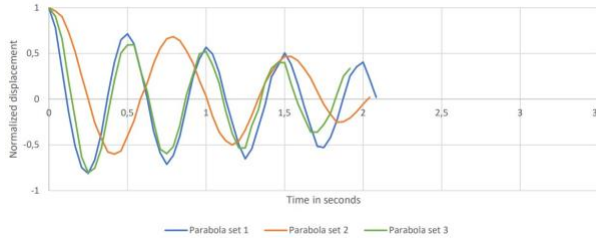

(b) after boom root actuation

Figure 24: Concept B tip deflection due to manual excitation (bending around x-axis) [10]

Both Figures show data from test with excitation deflections in y-direction that initiate vibrations around the boom x-axis. This axis is the one that is most effected from the stiffness reduction in the transition zone (see again Figure 3 on page 2. This is visualized well in Figure 24(a) as the boom tip never completed one full oscillation but only pan a bit back and forth to finally come to a stop at a random angle. Some rough estimation using the first half oscillations would results in oscillation periods about $3.0s$ to $3.5s$ and derived frequencies between $0.26Hz$ and $0.33Hz$. However, this could be only giving an impression of the order of magnitude and cannot considered to be a well-obtained result.

Once the boom root is deployed (see Figure 24(b)) the behaviour changes significantly. A clear characteristic of a damped vibrations can be recognized for the three graphs.

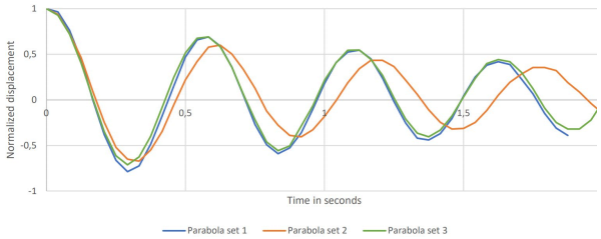

(a) before boom root actuation

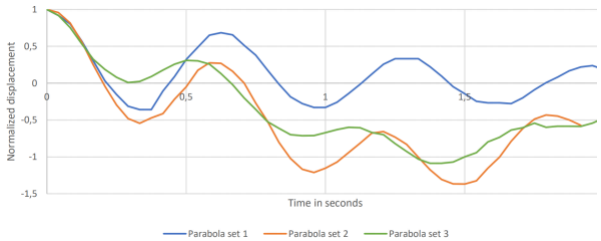

(b) after boom root actuation

Figure 25: Concept B tip deflection due to manual excitation (bending around y-axis) [10]

Figure 25 shows the same results for tests with excitation deflections in x-direction that initiate vibrations around the boom y-axis. In contrast to the analysis in the other direction a clear vibration pattern forms in the graphs even for the mechanism without deployed boom root. This results from the fact that the weakening of the bending stiffness is mainly impacting the bending around the x-axis. The bending stiffness around the y-axis is theoretically even higher in this region as the boom cross section is wider in x-direction.
However, due to the reduced stiffness in y-direction the vibrations in x-direction are strongly coupled with movements in y direction. Therefore, only the first parabola set (parabola #4) in Figure 25(a) could be analysed more in detail. The average period is about $0.64s$ resulting in an oscillation frequency of about $1.56Hz$.

in Figure 25(b) shows again a clear vibration characteristic and could be used to obtain vibration frequencies.

Table 3 compiles all swing-out test results for Concept B. The indexes in the top row variables indicate if the boom frequency f_B is measured on a *weak* boom with undeployed boom root or a *stiff* boom with deployed boom root. The Mx and My indicate if the boom was oscillation around its x or y axis (and previously excited with a torque around this axis).

All values written in round brackets could be only obtained by picking one full or even a half oscillation period and are therefore not considered reliable. However, when comparing the reliable value, $f_{B|stiff|Mx}$ obtained in parabola #10 attracts interest as the measured frequency was nearly cut in half while one would expect three nearly identical results for all the sets. Luckily, the footage of Cam #1 could provide insight into this massive drop in stiffness. Figure 26 compiles three similar images of this camera taken in each of the three sets after the boom root has been deployed. The two yellow dashed lines shall help to see the issue that is highlighted with the red ellipse. The root deployment at set 2 was initiated but not carried out to its full extend. While the difference in deployed width looks minor, it also suggests that the four boom root interface brackets (please refer again to Figure 8 on page 3) haven't reached their final positions and are therefore not fully locked into the spool. Due to the kinematic coupling of the root deployment and the locking of the spool in the outer structure, it is also probable

Table 3 Oscillation frequencies for Concept B

Parabolas	$f_{B\|weak\|Mx}/Hz$	$f_{B\|weak\|My}/Hz$	$f_{B\|stiff\|Mx}/Hz$	$f_{B\|stiff\|My}/Hz$
#4, #5 (Set 1)	(0.26)	1.49	2.1	1.9
#9, #10 (Set 2)	(0.33)	(1.7)	1.2	1.7
#14, #15 (Set 3)	(0.26)	(1.8)	2.1	1.8

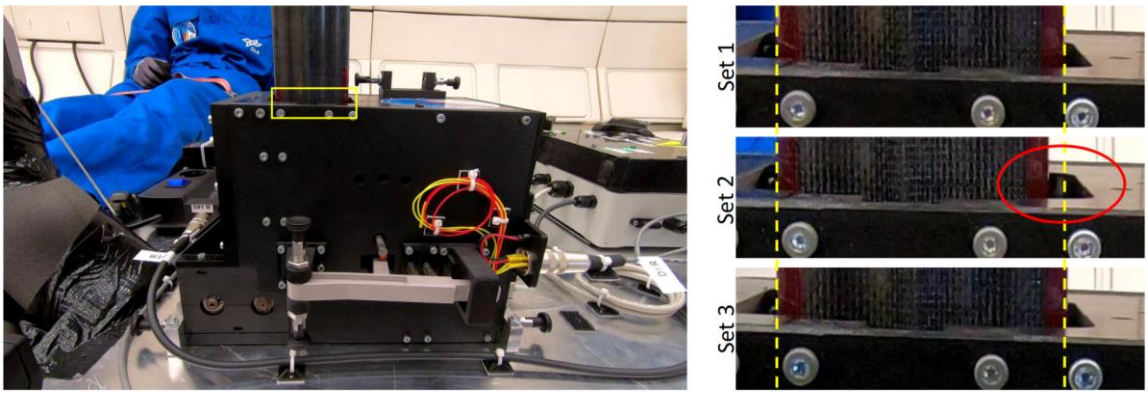

Figure 26: Deployed boom root of Concept B seen by Cam #1 for each of the last parabolas out of the three Concept B test sets (important spot is marked with a red ellipse)

that the spool is not firmly locked into the mechanisms side walls. Consequently, this few missing millimetres of deployment create a massive drop in stiffness.

9. CONCLUSION

All previously defined test objectives have been met. Both concepts demonstrated their operation under relevant environment and the test campaign was assessed to be a full success.

9.1. Concept comparison

Comparing both concepts, the prototype of *Concept A* was performing slightly better than *Concept B*. The expected increased stiffness of *Concept B* over *Concept A* could not be confirmed. *Concept A* oscillated at about $2.6Hz$ while *Concept B* could achieve $2.1Hz$. *Concept B* showed however the potential of its boom root deployment that increased the oscillation frequency of the boom by an order of magnitude once the root deployment was triggered.

One minor deployment failure was observed for *Concept B* while *Concept A* was operating without any problems. The very same *Concept A* mechanism was equipped with a $4.3m$ long boom in 2022. It preformed about 40-50 deployments and retractions under 1g at the ILA BERLIN Expo and the SPACE TECH EXPO Bremen. It is worth to mention that those demonstrations were done again with the $300\text{-}gram$ camera at the tip but no gravity compensation.

Nevertheless, the authors of this paper are convinced that the basic principles of *Concept B* will be able to push the stiffness much higher as observed with the here presented prototype. As stated above, the use of plastic parts is a valid approach for deployment mechanism prototypes and for the evaluation of the deployment it has served its purpose within this test series. However, when it comes to stiffness measurements, this material exchange can no longer be neglected.
Bending loads on the $2m$ long mast generate large individual force-pairs at the small boom support bracket in the mechanism, which must be absorbed by these small parts and the kinematics behind them. Some parts of these kinematics are still made from plastic in the current prototype. It is expected that a mechanism with stiffer components as well as a play-minimized design will generate a significant increase in stiffness. Thankfully, zero gravity will not be required for such stiffness tests on a new prototype. These tests will be performed in-house with existing test facilities.

9.2. Lessons learned on 0g testing

As always communicated by the service provider, a parabolic flight does not provide 0g but µ-g (micro-g). This is true for the vertical but also for the longitudinal and lateral aircraft axis. Thus, some movements of the deploying or deployed booms were influenced by lateral and longitudinal very small accelerations. Due to the lower bending stiffness, this effect was only observed for *Concept B*.

When performing dynamic tests like fast deployment or modal analysis on large lightweight structures, one other effect needs to be understood: The surrounding air adds a lot of damping to dynamic processes and thereby influences decay times as well as the deployment behaviour.

Concluding, parabolic flights provide a good option to test deployable structures in nearly perfect weightlessness. When planning such test, one should make sure that the small disturbances in g-level as well as the still present air can be tolerated or compensated.

For a further understanding of tests in this environment, three related papers for the remaining tests at this parabolic flight can be reviewed as well [6, 8, 9].

9.3. Test setup

As mentioned above, the focus of this test flight was to evaluate the proper operation of both concepts in weightlessness. The swing-out tests that were analysed by footage analysis were just considered a *low hanging fruit* that could be added easily to the test plan without any increase in test equipment. However, the not fully deployed boom root at parabola #10 may had remained undetected if the values in Table 3 hadn't raised interest. Moreover, the cause of the massive loss of stiffness could only be proven by the recorded footage of one of the five fixed cameras. This shows that it is essential for such experiments in a demanding environment to first collect as much measurement and camera data as possible in order to then search for correlations in quiet moments at the desk.

Concept B also proved that the vertical support mast and the safety rope were an important feature of the test setup. Without it, the mast of *Concept B* would have been bend over and severely damaged during the hyper-g phases.

9.4. Test rack electronics

Both Arduino-compatible control electronics worked as intended. The more complex electronics of *Concept B* did a good job in controlling the deployment mechanism respecting both user inputs and end-stop events. Moreover, it recorded relevant sensor data like from the IMU and the motor parameters (like current consumption, motor speed, etc.) very reliably on the internal SD-card memory.

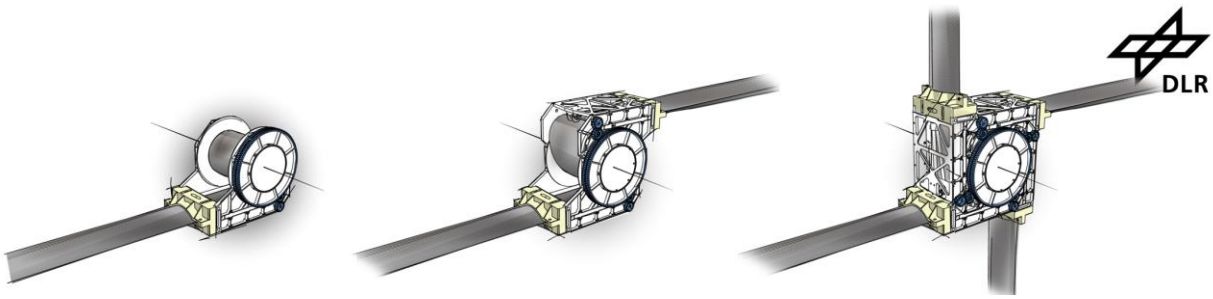

Figure 27: Modular, retractable boom deployment unit for 1, 2 or 4 booms

It is assumed that – if the operator is already used to C-programming – the use of such open source electronics is a good alternative to professional high-price data acquisition systems. The disadvantage for the inexperienced is clearly the programming via a complex programming language instead of a graphical user interface such as MATLAB Simulink or NI LabView. However, even with such environments, test benches are not programmed in a day and one is very often bound to the use of proprietary black-boxes whose internal function is neither explained in detail nor can be changed. For Arduino-software, every used library can be accessed, understood and modified if required.

For the operation of the here shown experiments in combination with the already existing c-programming skills of the operators, the decision for open-source electronics was never regretted.

10. OUTLOOK

The results of the test series have further strengthened our decision to focus on the floating core concept (*Concept A*) for further DLR developments in the field of high strain composite booms. In 2022 the concept was further streamlined to provide a scalable, modular and retractable concept for various deployable applications (see Figure 27).

Currently, a 4-boom deployment unit for membrane deployment is under development. A first engineering model design showed that it will be able to carry 4 booms up to $7m$ length each. The unit will fit the envelope of a 4-unit CubeSat (2x2x1) and should add a mass between 3 to $4kg$ to the spacecraft. Once the unit is integrated, combined boom bending and compression tests will be conducted with these mechanisms to finally determine how close the *Floating Core* concepts is to the ideal rigid interface.

11. ACKNOWLEDGMENTS

A significant credit is due to my master student Patrick Henkies, who completely reworked and improved the *Concept B* deployment mechanism for the parabolic flight. He also built and programmed the control electronics from scratch and evaluated the test afterwards and documented it well in his master thesis [10].

Moreover, we would like to thank our institute director Professor Martin Wiedemann, our department head Professor Christian Hühne as well as the team of NOVESPACE for their full support.

12. REFERENCES

[1] Straubel, M., *Design and Sizing Method for Deployable Space Antennas,* Ph.D. thesis, Otto-von-Guericke-Universität Magdeburg, GERMANY, Sep 2012. URL http://elib.dlr.de/81128/.

[2] Straubel, M., Hillebrandt, M., and Hühne, C., *Evaluation of Different Architectural Concepts for Huge Deployable Solar Arrays for Electric Propelled Space Crafts*, 14th European Conference on Spacecraft Structures, Materials and Environmental Testing, Toulouse, France, 2016

[3] Hillebrandt, M., Zander, M. E., and Hühne, C., *Apparatus for Unfolding a Mast*, U.S. Patent 10 717 628, July 21, 2020.

[4] Straubel, M., *Vorrichtung und Verfahren zum entfalten eines aufgerollten länglichen Hohlkörpers*, U.S. Patent Application Publication No. 2020/0324921 A1, October 15, 2020

[5] Hillebrandt, M., Zander, M. E., and Hühne, C., *Sliding Core Deployment Mechanism for Solar Sails based on Tubular Shell Masts*, Proceedings of 5th International Symposium on Solar Sailing, 2019. URL https://elib.dlr.de/129630/

[6] Hillebrandt, M., Meyer, S., Stegmaier, M., Straubel, M., Zander, M. E., and Hühne, C., *Zero-G Deployment Testing of a New Rollable and Retractable Solar Array*, AIAA SciTech 2023, National Harbor, MD, USA, 2023.

[7] Straubel, M., and Hühne, C., *CTM Boom Deployment Mechanism with Integrated Boom Root Deployment for Increased Stiffness of the Boom-to-Spacecraft Interface*, *European Conference on Spacecraft Structures, Materials and Environmental Testing (ECSSMET 2021)*, 2021. URL https://elib.dlr.de/141680/.

[8] Richter, M., Straubel, M., Zander, M. E., Salazar, J., Chamberlain, M., and Fernandez, J., *Force Application of a Single Boom for a 500-m2-Class Solar Sail*, *AIAA SciTech 2023*, National Harbor, MD, USA, 2023.
[9] Zander, M. E., Chamberlain, M., Jost, D., Müller, D., Hagmeister, N., Straubel, M., and Hühne, C., *Design and Testing of the BionicWingSat in a Zero-g Flight Campaign - A 2U-CubeSat with Deployable, Biologically-Inspired Wings*, *AIAA SciTech 2023*, National Harbor, MD, USA, 2023.
[10] Henkies, P., *Design of a GOSSAMER-1 type boom deployment mechanism with increased boom root stiffness*, Master's thesis, University of Applied Sciences Aachen, September 2021.